communications engineering

A Nature Portfolio journal

Article

https://doi.org/10.1038/s44172-025-00551-x

Thermal stability enhancement of low temperature Cu-Cu bonding using metal passivation technology for advanced electronic packaging

Mu-Ping Hsu[1,3], Tai-Yu Lin[1,3], Hua-Jing Huang[2], Chiao-Yen Wang[1], Tsai-Fu Chung[2], Wen-Wei Wu[2] & Kuan-Neng Chen[1] ✉

This work investigates the thermal stability of Cu-Cu bonding using a thin Ag passivation layer in applications targeting advanced packaging. Conventional Cu-Cu bonding often requires elevated temperatures (≥250 °C) that can exacerbate thermal stress and limit process flexibility, making multi-chip stacking more challenging. By introducing a 3 nm Ag passivation layer, we demonstrate reliable bonding at lower temperatures with improved durability against high-humidity and high-temperature environments, as confirmed by both Highly Accelerated Stress Tests (HAST) and burn-in measurements. In-situ transmission electron microscopy (TEM) and 4D-STEM strain mapping reveal that Ag diffusion along Cu grain boundaries not only retards abnormal grain growth but also reduces interfacial void formation at elevated temperatures. These enhancements collectively maintain a stable interface and superior mechanical strength relative to that for non-passivated Cu-Cu bonding. The results highlight the importance of metal passivation in enabling low-temperature Cu-Cu bonding technologies with robust thermal stability, providing the feasibility for next-generation advanced packaging platforms.

Recent advancements in 3D integration technologies such as TSMC's SoIC, Intel's EMIB, and Samsung's X-Cube highlight the importance of advanced packaging in enhancing high-performance computing (HPC)[1–4]. Integrating more compute chiplets, high bandwidth memory (HBM), co-packaged optics (CPO), and passive devices can address bandwidth, power delivery, and signal integrity challenges, as illustrated in Fig. 1 The above scenarios rely heavily on sequential stacking technology, such as HBM and chiplet integration, indicating that a robust bonding should feature a low thermal budget, short bonding duration and good thermal stability to prevent issues from repeated heating and cooling cycles during sequential stacking. Conventional solder-based stacking technology, although widely used, faces critical scaling challenges in smaller pitches. Problems such as solder squeezing, electromigration, and high reflow temperatures (260 °C) adversely affect both reliability and electrical performance[5–7]. In response, Cu-Cu bonding has gained attraction in support of high-density interconnects because copper offers excellent electrical conductivity, robust thermal dissipation, and potential for finer-pitch scalability. However, copper surfaces oxidize readily, often requiring elevated bonding temperatures of 250–400 °C[8–12]. These high temperatures can induce thermal stress, delamination, and additional complexity in sequential chip stacking.

To mitigate these issues, researchers have proposed multiple methods to reduce the required bonding temperature, including acid-based surface treatments[13,14], the use of self-assembled monolayers[15,16], plasma activation[17–19], and the use of nanocrystalline[20,21] or nano-twinned copper films[22–24]. Among these techniques, metal passivation bonding has demonstrated the most pronounced temperature reduction, achieving bonding below 120 °C in ambient conditions using less than 1 min[25–28]. Metal passivation bonding is also the only technology that is not constrained by bond size and pitch. Table 1 summarizes the bonding conditions of the Cu-Cu bonding candidates. Passivation bonding differs from other Cu-Cu bonding technologies in two key ways. First, a passivation metal such as Ag or Au is deposited onto the Cu surface to prevent oxidation. Second, Cu atoms diffuse more readily through the grain boundaries of the passivation layer, as illustrated in Fig. 2, reducing the time and temperature needed for a strong bond[25,29,30]. In contrast, other Cu-Cu bonding technologies typically

[1]Institute of Electronics, National Yang Ming Chiao Tung University, Hsinchu, Taiwan. [2]Department of Materials Science and Engineering, National Yang Ming Chiao Tung University, Hsinchu, Taiwan. [3]These authors contributed equally: Mu-Ping Hsu, Tai-Yu Lin. ✉e-mail: knchen@nycu.edu.tw

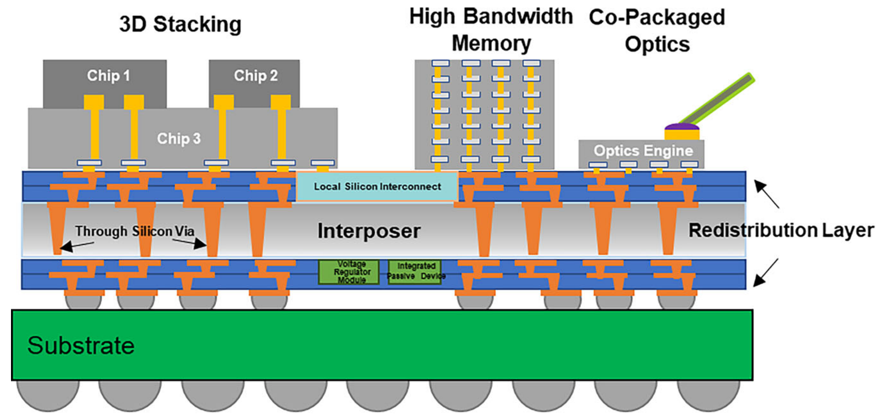

Fig. 1 | Conceptual diagram of the advanced packaging. Advanced packaging based on Cu-Cu bonding techniques can increase function density by integrating high bandwidth memories, high-performance computing, Co-Packaged Optics (CPO), and even passive device.

Table 1 | Comparison of Cu-Cu bonding

Candidates	Cu-Cu[10–13,33,44–46]	Nanocrystalline Cu[20,21,47]	Nano-twin[22–24,48–52]	Passivation[25–28]	
Scheme	W2W / D2D	D2W / D2D	W2W / D2D	W2W / D2D	
Bonding temperature	250 °C	300 °C	150 °C	R.T.	70 °C
Bonding duration	3 min	10–40 min	60 min	50 min	1 min
Post annealing	w/o	w/o	w/o	100 °C (10–60 min)	w/o
Pad (<3 um)	N/A	N/A	N/A	N/A	available

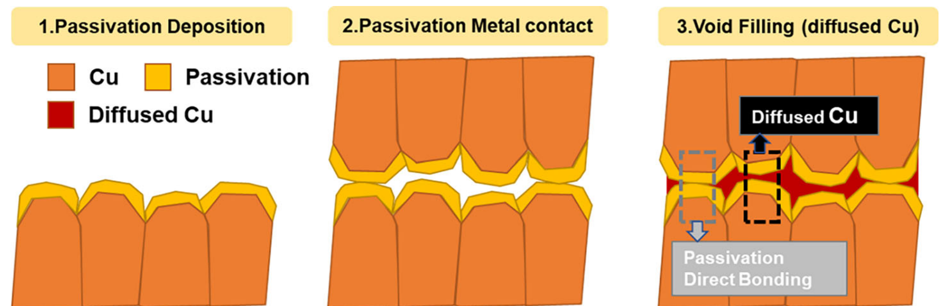

Fig. 2 | Mechanism of passivation bonding. Passivation bonding prevents Cu oxidation and facilitates lower-temperature Cu atom diffusion through grain boundaries, effectively reducing bonding temperature and enhancing interfacial integrity.

rely on the lattice diffusion of copper atoms, which requires higher temperatures and longer bonding durations[16,31,32].

Although passivation bonding enables Cu-Cu interconnections to be formed at lower temperatures and in shorter times, its thermal stability has not been thoroughly investigated in previous studies. Moreover, even conventional high-temperature Cu-Cu bonding lacks comprehensive verification of thermal stability during sequential stacking. Given the evolving trends in the advanced packaging industry, there is a critical need for bonding technologies that offer both low-temperature processing, short bonding duration, and robust thermal stability. This investigates the thermal stability of conventional Cu-Cu bonding and Cu-Cu bonding that employs a metal passivation layer, considering both macroscopic and microscopic perspectives. At the macroscopic level, we measure mechanical strength and electrical performance during stress tests and extended annealing, generating insights into the reliability of the bonded structures. On the microscopic level, we use in-situ transmission electron microscopy (TEM) to examine interfacial changes such as grain coarsening, void nucleation, and passivation metal clustering at elevated temperatures. This integrated viewpoint elucidates the mechanisms behind thermal degradation and guides the optimization of passivation strategies for improved bond robustness. Ultimately, these findings are expected to facilitate the development of reliable low-temperature Cu-Cu interconnects suitable for multi-chip stacking in next-generation advanced packaging platforms.

Methods

This work explores two bonding structures: Cu-Cu bonding with and without metal passivation, both on a 4-inch Si wafer featuring an SiO_2 insulation layer, a Ti adhesion layer, and a Cu conduction layer, as well as an additional 3 nm Ag layer for passivation, as shown in Supplementary Fig. 1. The fabrication process began with RCA cleaning of the Si substrate to remove contaminants and particles, followed by the deposition of a SiO_2 layer to serve as an insulating or passivating film. Next, photoresist (PR) was applied to the SiO_2 layer to create a mask for subsequent patterning, after which a metal stack comprising 30 nm Ti, 300 nm Cu, and 3 nm Ag was deposited onto the exposed areas using physical vapor deposition (DC-sputtering, Ion Tech Microvac 450CB) at a deposition rate of 1 Å/s under a working pressure of 4×10^{-6} torr. The PR was then stripped using a lift-off technique, leaving the metal in the desired pattern on the SiO_2 surface. After the above process, surface roughness measurements were conducted, as the roughness of the bonding surface is crucial for bonding quality. The Cu surface of the Cu-Cu bonding samples exhibited a surface roughness (Ra) of approximately 1.36 nm, while the Cu-Cu bonding samples with Ag passivation showed a slightly higher Ra value of 1.55 nm, as shown in Fig. 3. These results indicate that both surfaces were sufficiently smooth to support high-quality bonding. Then, the wafers were subsequently diced into 5 mm × 5 mm top dies and 10 mm × 10 mm bottom dies. Then Cu-Cu bonding samples were successfully bonded at 250 °C under ambient air for

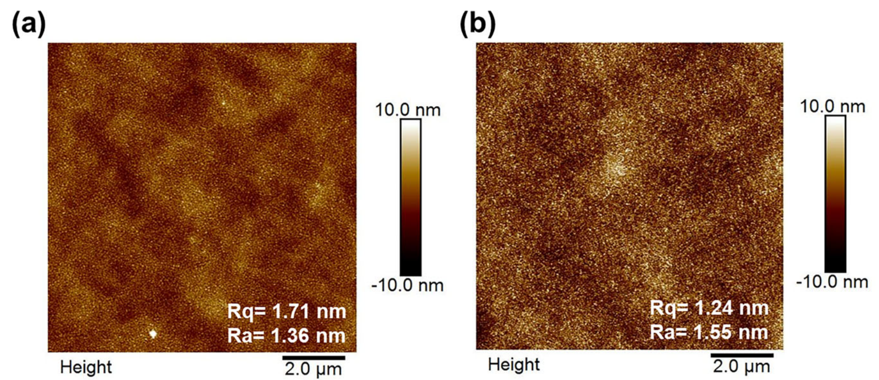

Fig. 3 | Surface roughness of samples before bonding. **a** The Cu-Cu bonding samples and (**b**) the Cu-Cu bonding samples with Ag passivation.

180 s with 7.85 MPa applying force, while the dies with Ag passivation were successfully bonded at 180 °C for 60 s under ambient air with 7.85 MPa applying force. Both bonding structures employed Kelvin structures with a 50 μm × 50 μm bonding pad to measure electrical characteristics (Supplementary Fig. 1). This study evaluates the thermal stability of bonded structures from both macroscopic and microscopic perspectives. At the macroscopic level, specimens underwent an unbiased, highly accelerated stress test (HAST) at 110 °C and 85% relative humidity for 264 h in accordance with JESD22-A118, followed by contact-resistance measurements. Mechanical strength and electrical performance were further assessed after extended high-temperature annealing at 180 °C for 8 h and 300 °C for 50 min. At the microscopic level, in-situ transmission electron microscopy (TEM) was used to monitor interfacial evolution at elevated temperatures. TEM lamellae were prepared by focused ion beam (FIB), and a protective layer was first deposited on the bonded samples to mitigate Ga^+ damage, and controlled the lamella thickness to about 100 nm to enable high-resolution imaging. The specimen was then transferred with a glass tip onto an in situ TEM heating chip and mounted on a Protochips Fusion Select holder (Aduro 300) for dynamic observation, as illustrated in Supplementary Fig. 5.

Results and Discussion

Thermal stability bonding structure investigation

To first evaluate the bonding quality of both structures, both Cu-Cu bonding structure and passivation structure were sent for HAST. Before HAST, the contact resistance of Cu-Cu bonding with and passivation structure was approximately 2.02×10^{-7} Ω·cm² and 2.55×10^{-7} Ω·cm², respectively. After 264 h of unbiased HAST, both samples without any underfill protection (which is typically used to protect solder bumps) maintained stable bonding and exhibited only minor deterioration in specific contact resistance, 4% deterioration for the passivated sample and 8% deterioration for the non-passivated one, as shown in Fig. 4a, b These results indicate that the both bonded structures were well bonded and could withstand severe humidity and temperature variations without obvious degradation of electrical performance.

To further investigate the thermal stability of the bonding structure, a burn-in test was performed, involving heating the samples under a nitrogen atmosphere without electrical current as an accelerated aging process. Electrical performance was evaluated before and after annealing at 180 °C for 8 h (Supplementary Fig. 5) and at 300 °C for 50 min, as shown in Fig. 4c–e. The Ag passivation structure showed stable electrical performance, exhibiting only a slight increase of about 2.8 % in contact resistance after 8 h at 180 °C. After annealing at 300 °C for 50 min, the contact resistance decreased by 6%. In contrast, Cu-Cu bonding without passivation experienced a small change in contact resistance about 3% after 8 h at 180 °C, indicating moderate stability. However, it failed after exposure to 300 °C for 50 min, revealing insufficient thermal stability at higher temperatures. Furthermore, Fig. 4f shows that after annealing for 60 to 240 min, the mechanical strength of Cu-Cu bonding with metal passivation initially increased and then plateaued, while that without passivation gradually declined. The Cu-Cu bonding with passivation maintained superior mechanical strength compared to that without passivation in all cases.

Previous investigations reported that Cu-Cu bonding at or above 400 °C, followed by annealing at the same temperature, was shown to obviously improve interfacial morphology through increased grain growth and elimination of voids[12,33–35]. Such high-temperature conditions provide sufficient thermal energy for interatomic diffusion and recrystallization, thereby reinforcing the bond. However, in low-temperature bonding scenarios (below 250 °C), post-bonding annealing typically offers fewer benefits due to incomplete grain growth and recrystallization of the bonding interface. Furthermore, incomplete grain growth and recrystallization at the bonding interface have the opportunity to allow cracks to propagate along regions of 'poor', non-saturated grain growth, ultimately weakening the bonding strength. In this study, both the Cu-Cu bonding structure and the passivation structure were bonded at lower temperatures and shorter durations. It is reasonable to assume that the bonding interface of the Cu-Cu bonding structure in this case is incomplete grain growth and recrystallization. However, after passivation is applied, both electrical performance and bonding strength can be effectively improved under low bonding temperature and short bonding duration, suggesting that passivation at the bonding interface helps reduce the consequences of incomplete grain growth and recrystallization. (Supplementary Note 2-Bonding mechanism of passivation bonding).

In-Situ TEM analysis of microstructure transformation

In-situ TEM analysis (Supplementary Note 3- Experimental setup before In-situ TEM analysis.) was conducted to observe the real-time behavior of Cu-Cu bonding structures and passivation structures, under controlled thermal conditions. The bonded samples were prepared as in-situ TEM specimens using a focused ion beam (FIB) system equipped with SEM and were then placed on a temperature-controlled holder for simultaneous heating and microscopic examination. The temperature profile for the in-situ TEM experiment and the corresponding times are labeled in the figures, as shown in Figs. 5a, 6a, and 7a. The temperature profile starts from the room temperature, and then the temperature increases to around 180 °C, marking the first plateau (labeled as 1). After a hold period of 90 min, the temperature rises again to 300 °C (labeled as 2) and is held for 50 min. Finally, the temperature increases to about 400 °C (labeled as 3) for 20 min.

Before the in-situ TEM experiment, both Cu-Cu bonding structures and the passivation structures were well bonded which had been verified by measuring the contact resistance and also evaluated by TEM analysis as shown in Figs. 5b, 6b. Notably, very few voids can be observed at the Cu-Cu bonding interface. To investigate how the incomplete grain growth and recrystallization of the bonding interface affect bonding quality after thermal stress, we selected the area with voids for subsequent in-situ TEM observation as shown in Fig. 5c–e. Furthermore, for the passivation structure, the void-free bonding interface was formed by passivation direct bonding and Cu-diffused area (Supplementary Note 2-Bonding mechanism of passivation bonding). Therefore, the in-situ TEM observation area was

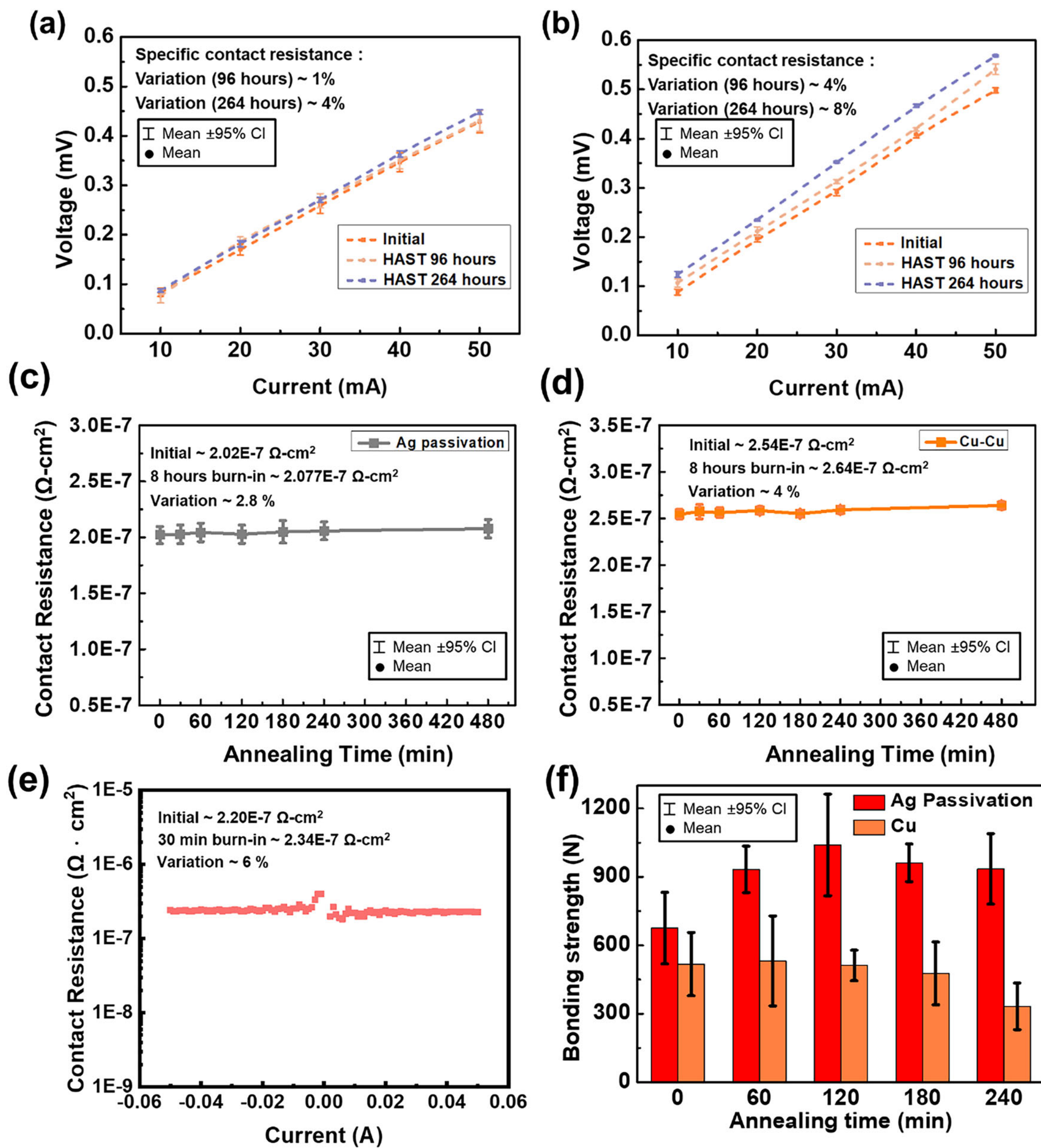

Fig. 4 | Electrical performance before and after HAST of boned samples. **a** passivation structure and (**b**) Cu-Cu bonding. Electrical performance before and after 180 °C burin-in of (**c**) passivation structure (**d**) Cu-Cu bonding. **e** Electrical performance after 300 °C burin-in of passivation structure. **f** Mechanical strength after 180 °C burin-in of with and without passivation structure.

selected at the region consisting of a passivation direct bonding area and a Cu-diffused area as shown in Fig. 6c.

During the initial isothermal hold at 180 °C for 90 min, at low magnification, most bonded area of both the bare Cu-Cu bonding and the passivation bonding structures exhibited obvious thermal stability, as shown in Figs. 5f, g and 6d. However, clustering of adjacent voids was observed within the Cu-Cu bonding interface at high-resolution TEM as shown in Fig. 5h. The observations confirmed that low-temperature Cu-Cu bonding does not benefit from post-bonding annealing. Moreover, it is reasonable to assume that the clustering of adjacent voids at the bonding interface during heating has the chance to allow cracks to propagate along the bonding interface, ultimately weakening the bonding strength, as the pull test results shown in Fig. 4f.

In the passivation samples, as shown in Fig. 7a–f, two notable phenomena were identified through HR-TEM: First, at the passivation direct bonding area, the aggregation of passivation metal within the passivation layer was observed during heating, as shown in Fig. 7e. The observed aggregation of the passivation metal during heating is attributed to agglomeration phenomena, which are well-documented in metal thin films under thermal stress. As supported by literature[36], agglomeration in silver thin films is primarily driven by surface diffusion processes that become active at elevated temperatures. These processes cause the film to minimize its surface energy by forming clusters, leading to discontinuities such as voids or hillocks. Although the passivation metal migrated during heating, diffused Cu simultaneously filled the vacated spaces, thereby maintaining a dynamic equilibrium at the bonding interface and keeping it void-free. Second, diffused Cu at the bonding interface would recrystallize during heating, and then the bonding interface would gradually vanish. Therefore, the aggregation of the passivation metal, coupled with the diffusion of Cu atoms into the vacated regions, maintained a dynamic equilibrium that preserved a void-free interface. As a result, the bonded samples exhibited stable electrical performance and mechanical strength after aging.

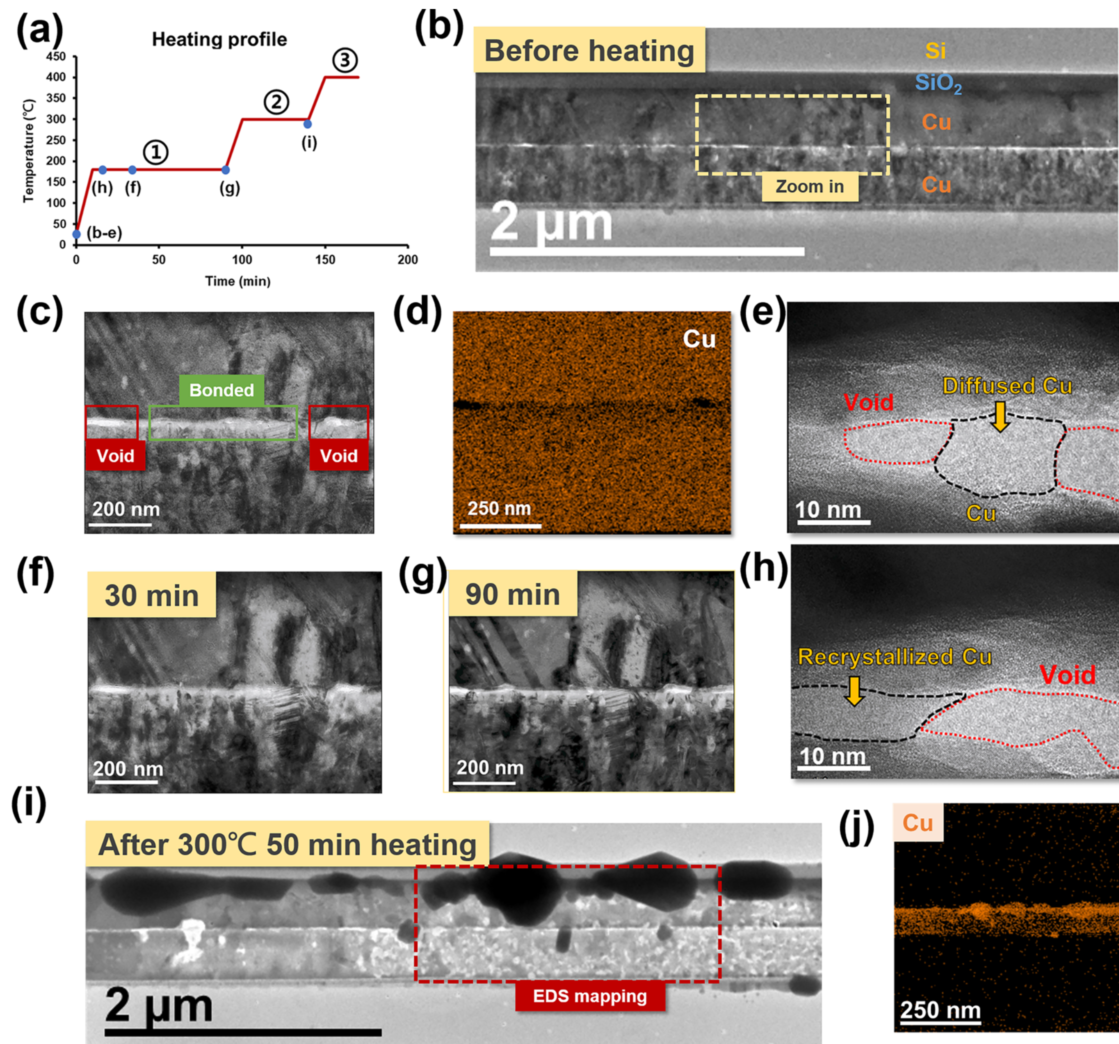

Fig. 5 | Heating profile of in-situ TEM and in-situ TEM results of Cu-Cu bonding interface. a Heating profile of in-situ TEM. **b** In-situ TEM images of Cu-Cu bonding interface (before heating). **c** Selected area for In-situ TEM, including well-bonded and void area. **d** EDS of the selected area (before heating). **e** HR-TEM image of the selected area (before heating). **f** In-situ TEM image of sample after 180 °C heating for 30 min. **g** In -situ TEM images of sample after 180 °C heating for 90 min. **h** Merging of the adjacent voids of the Cu-Cu bonding interface after 180 °C heating for 10 min. **i** In-situ TEM images of Cu-Cu bonding interface after 300 °C heating for 50 min. **j** EDS of Cu-Cu bonding interface after 300 °C heating.

Upon further heating to 300 °C, the bare Cu-Cu bonding structure exhibited pronounced abnormal grain growth and numerous voids, as shown in Fig. 5i, j. In contrast, the passivation structure showed only minor grain growth at the interface as shown in Fig. 6e, g. Even at 400 °C, the passivated sample remained relatively stable, as shown in Fig. 6f, h. These findings, combined with the burn-in testing results, which revealed the importance of incorporating a passivation layer for low-temperature Cu-Cu bonding.

On the basis of the results in this study, the passivation layer obviously enhances the thermal stability and mechanical performance of Cu-Cu bonding structures, which may be attributed to the diffusion of Ag atoms into Cu grain boundaries during annealing and therefore forming a solid solution and contributing to grain boundary segregation strengthening. This process reduces the grain boundary energy and impedes the movement of dislocations, thereby improving structural integrity under thermal stress, which has been validated[37]. Furthermore, several studies reveal that doping multiple metals can reduce abnormal grain growth[38–41]. In this study, the Ag passivation layer stabilizes the microstructure by limiting abnormal grain growth at elevated temperatures. Without the use of passivation, abnormal grain growth often leads to void formation and interfacial degradation. The Ag layer controls the movement of the Cu atom and ensures more uniform grain growth, which is critical for maintaining a consistent and reliable interface during prolonged thermal exposure[30,42,43].

These combined effects explain the results that Cu-Cu bonding structures with a Ag passivation layer consistently outperform bare Cu-Cu bonding in high-temperature applications, as observed in both in-situ TEM and burn-in tests. The Ag passivation layer not only improves contact resistance under thermal stress but also prevents failure at elevated temperatures, making it particularly valuable in low-temperature bonding applications where thermal budget constraints limit the benefits of post-bonding annealing.

4D-STEM strain mapping of the microstructure

To observe Ag segregation at Cu grain boundary, 4D-STEM strain mapping was employed. This technique enabled the detection of changes in stress distribution, providing insights into the grain boundary diffusion mechanisms of the bonding materials, and supplementing observations not accessible through EDS. As a method with enhanced sensitivity and spatial resolution, 4D-STEM allows the detection of variations in lattice constants in both real and reciprocal space, facilitating the precise measurement of internal stresses within metallic materials.

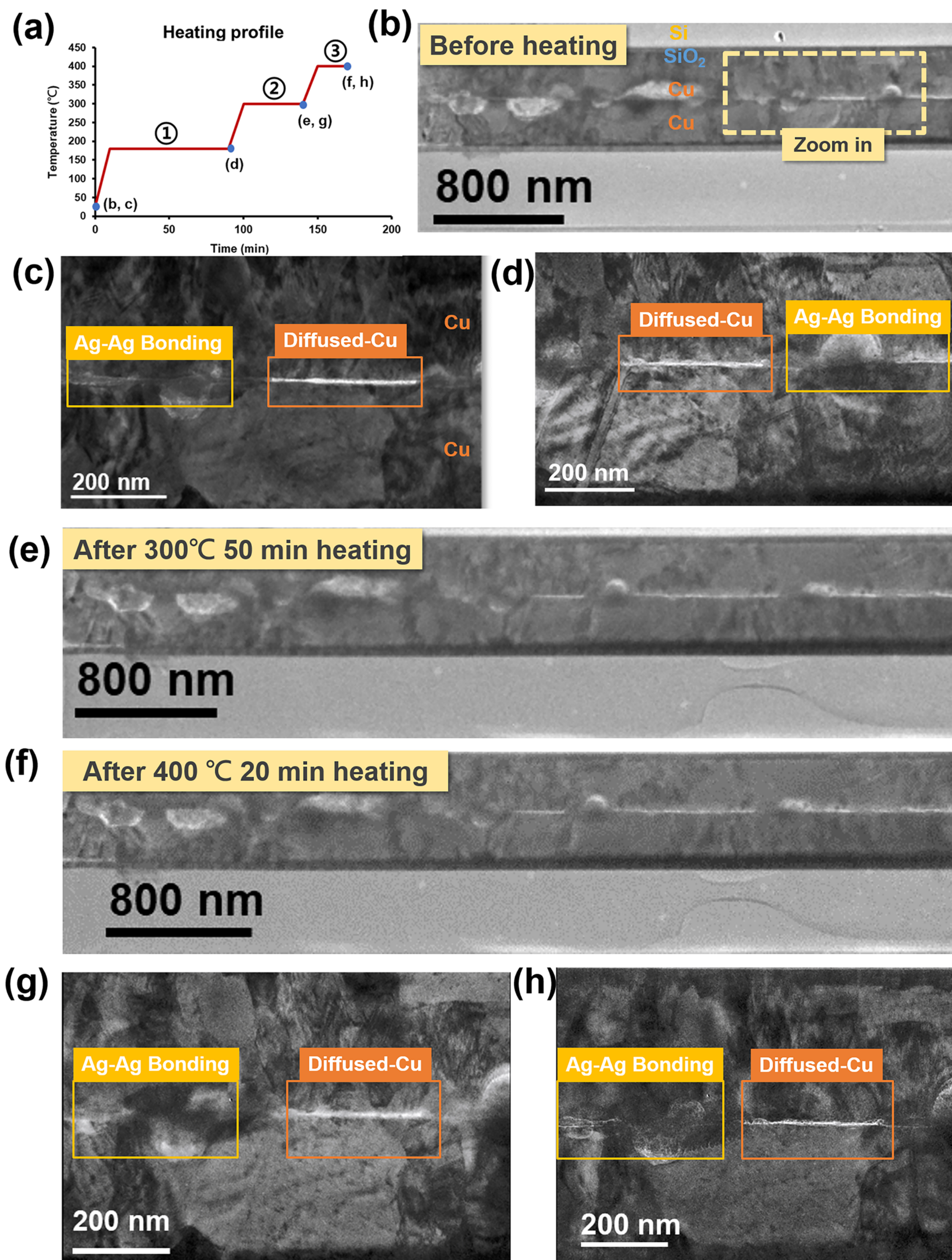

Fig. 6 | Heating profile of in-situ TEM and in-situ TEM results of the passivation bonding interface. a Heating profile of in-situ TEM. **b** TEM images of the passivation bonding interface (before heating). **c** Selected area for In-situ TEM, including passivation direct bonding and Cu-diffused area. **d** In-situ TEM images of selected area after 180 °C heating for 90 min. **e** TEM images of passivation bonding interface after 300 °C heating for 50 min. **f** TEM images of passivation bonding interface after 400 °C heating for 20 min. **g** In-situ TEM images of selected area after 300 °C heating for 50 min. **h** In-situ TEM images of selected area after 400 °C heating for 20 min.

Before annealing, the analysis of the passivation structure using 4D-STEM revealed a distinct boundary between the Cu thin film and the Ag passivation layer. As illustrated in Fig. 8a, the bulk Cu region served as the reference point for stress mapping. The Ag regions within the passivation structure exhibited compressive strain as a result of the larger lattice constant of Ag compared to Cu.

The post-annealing results, depicted in Fig. 8b, demonstrated obvious alterations in the stress distribution at the bonding interface. The compressive strain observed at the Cu grain boundaries and passivation direct bonding regions suggests that Ag atoms diffused into the grain boundaries of Cu and segregated, as indicated by the black solid-outlined area. This diffusion is consistent with the mechanism in which the grain boundary disorder facilitates atomic migration, enhancing the bond integrity of the passivated structure after thermal treatment[37]. Comparison of the pre- and post-annealing states clearly indicates that passivation atoms diffuse through the Cu grain boundaries, contributing to improved bonding stability.

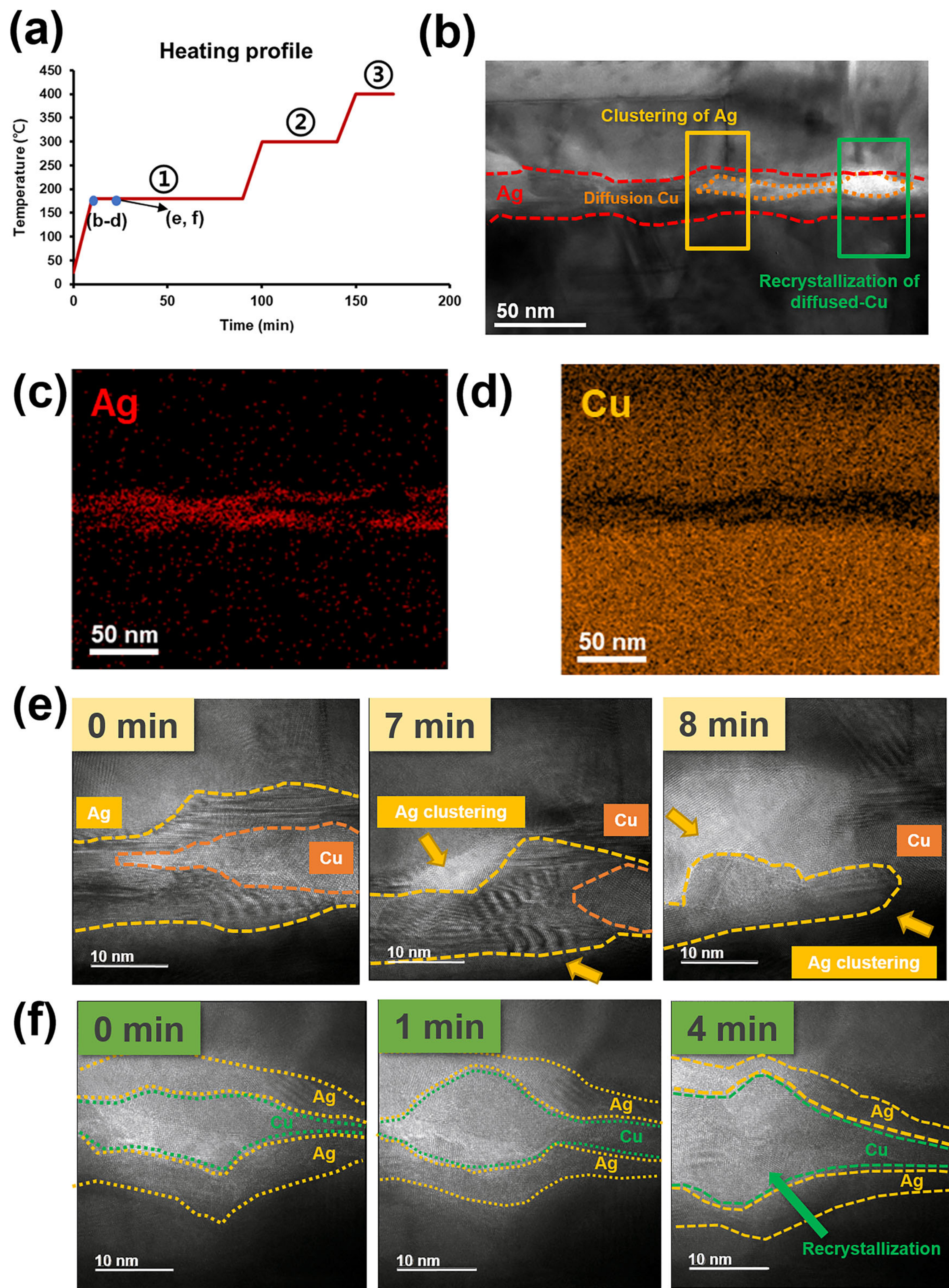

Fig. 7 | Heating profile of in-situ TEM and HR-TEM results of passivation bonding interface. **a** Heating profile of in-situ TEM. **b** HR-TEM images of passivation bonding interface before heating. EDS of the selected area before heating (**c**) Ag and (**d**) Cu. **e** In-situ TEM images of passivation clustering during 180 °C heating. **f** In-situ TEM images of recrystallization during 180 °C heating.

Conclusion

This study demonstrates that incorporating an Ag passivation layer substantially enhances the thermal stability and mechanical robustness of low-temperature Cu-Cu bonding. Specifically, electrical measurements under HAST and burn-in tests confirmed that Ag passivation effectively mitigates deterioration in contact resistance and prevents interfacial failure at higher annealing temperatures. In-situ TEM observations further revealed that the Ag passivation layer suppresses abnormal grain growth and facilitates more uniform Cu diffusion at elevated temperatures, thereby reducing void formation and improving interfacial integrity. An additional 4D-STEM strain mapping corroborated that Ag atoms diffuse along Cu grain boundaries, contributing to grain boundary strengthening. Collectively, these findings

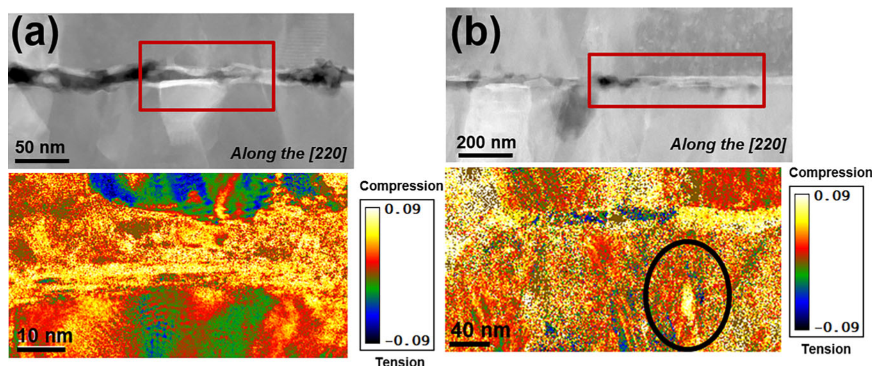

Fig. 8 | 4D-STEM strain mapping images of passivation structure. (**a**) before annealing (**b**) after 180 °C for 8 h annealing.

show that metal passivation not only reduces the bonding temperature but also ensures reliable long-term performance for advanced packaging, addressing the challenges posed{Citation} by repeated thermal cycling and miniaturized pitch requirements.

Data availability

All data supporting the findings of this study are available from the corresponding author upon reasonable request.

Received: 12 April 2025; Accepted: 6 November 2025;
Published online: 13 December 2025

References

1. Lin, X.-W. et al. Heterogeneous Integration Enabled by the State-of-the-Art 3DIC and CMOS Technologies: Design, Cost, and Modeling. in *2021 IEEE International Electron Devices Meeting (IEDM)*, San Francisco, CA, USA: IEEE, Dec. 2021, p. 3.4.1–3.4.4.
2. Bhattacharya, S. et al. Advanced System in Package Enabled by Wafer Level Heterogeneous Integration of Chiplets. in *2022 International Electron Devices Meeting (IEDM)*, San Francisco, CA, USA: IEEE, Dec. 2022, p. 3.1.1–3.1.4.
3. Cao, L. Advanced Packaging Technology Platforms for Chiplets and Heterogeneous Integration. in *2022 International Electron Devices Meeting (IEDM)*, San Francisco, CA, USA: IEEE, Dec. 2022, p. 3.3.1–3.3.4.
4. Hou, S.Y. et al. Integrated Deep Trench Capacitor in Si Interposer for CoWoS Heterogeneous Integration. in *2019 IEEE International Electron Devices Meeting (IEDM)*, San Francisco, CA, USA: IEEE, Dec. 2019, p. 19.5.1–19.5.4.
5. Zhan, C.-J., Chuang, C.-C., Juang, J.-Y., Lu, S.-T. & Chang, T.-C. Assembly and reliability characterization of 3D chip stacking with 30μm pitch lead-free solder micro bump interconnection. in *2010 Proceedings 60th Electronic Components and Technology Conference (ECTC)*, Las Vegas, NV, USA: IEEE, 2010, pp. 1043–1049.
6. Zhan, C.-J. et al. Development of fluxless chip-on-wafer bonding process for 3DIC chip stacking with 30μm pitch lead-free solder micro bumps and reliability characterization. in *2011 IEEE 61st Electronic Components and Technology Conference (ECTC)*, Lake Buena Vista, FL, USA: IEEE, May 2011, pp. 14–21.
7. Zhang, Z. & Wong, C. P. Recent Advances in Flip-Chip Underfill: Materials, Process, and Reliability. *IEEE Trans. Adv. Packag.* **27**, 515–524 (2004).
8. Gattinoni, C. & Michaelides, A. Atomistic details of oxide surfaces and surface oxidation: the example of copper and its oxides. *Surf. Sci. Rep.* **70**, 424–447 (2015).
9. Platzman, I., Brener, R., Haick, H. & Tannenbaum, R. Oxidation of Polycrystalline Copper Thin Films at Ambient Conditions. *J. Phys. Chem. C.* **112**, 1101–1108 (2008).
10. Tan, C. S., Peng, L., Li, H. Y., Lim, D. F. & Gao, S. Wafer-on-Wafer Stacking by Bumpless Cu–Cu Bonding and Its Electrical Characteristics,. *IEEE Electron Device Lett.* **32**, 943–945 (2011).
11. Rebhan, B. et al. Low-Temperature Cu-Cu Wafer Bonding. *ECS Trans.* **50**, 139–149 (2013).
12. Chen, K. N., Fan, A., Tan, C. S., Reif, R. & Wen, C. Y. Microstructure evolution and abnormal grain growth during copper wafer bonding. *Appl. Phys. Lett.* **81**, 3774–3776 (2002).
13. Kim, J.-W., Jeong, M.-H. & Park, Y.-B. Effect of HF & H2SO4 pretreatment on interfacial adhesion energy of Cu–Cu direct bonds. *Microelectron. Eng.* **89**, 42–45 (2012).
14. Yang, W., Shintani, H., Akaike, M. & Suga, T. Low temperature Cu-Cu direct bonding using formic acid vapor pretreatment. in *2011 IEEE 61st Electronic Components and Technology Conference (ECTC)*, Lake Buena Vista, FL, USA: IEEE, May 2011, pp. 2079–2083.
15. Lim, D. F., Wei, J., Ng, C. M. & Tan, C.S. Low temperature bump-less Cu-Cu bonding enhancement with self assembled monolayer (SAM) passivation for 3-D integration. in *2010 Proceedings 60th Electronic Components and Technology Conference (ECTC)*, Las Vegas, NV, USA: IEEE, 2010, pp. 1364–1369.
16. Tan, C. S., Lim, D. F., Singh, S. G., Goulet, S. K. & Bergkvist, M. Cu–Cu diffusion bonding enhancement at low temperature by surface passivation using self-assembled monolayer of alkane-thiol. *Appl. Phys. Lett.* **95**, 192108 (2009).
17. Chiang, C.-C. et al. Effects of O_2 - and N_2 -Plasma Treatments on Copper Surface. *Jpn. J. Appl. Phys.* **43**, 7415–7418 (2004).
18. Hu, L. et al. Multi-Die to Wafer Bonding Through Plasma-Activated Cu-Cu Direct Bonding in Ambient Conditions. in *2021 IEEE International 3D Systems Integration Conference (3DIC)*, Raleigh, NC, USA: IEEE, Oct. 2021, pp. 1–5.
19. Hu, L. et al. In-Depth Parametric Study of Ar or N2 Plasma Activated Cu Surfaces for Cu-Cu Direct Bonding. in *2021 IEEE 71st Electronic Components and Technology Conference (ECTC)*, San Diego, CA, USA: IEEE, June 2021, pp. 420–425.
20. Jhan, J.-J., Wataya, K., Nishikawa, H. & Chen, C.-M. Electrodeposition of nanocrystalline Cu for Cu-Cu direct bonding. *J. Taiwan Inst. Chem. Eng.* **132**, 104127 (2022).
21. Li, C.-N., Chiu, W.-L. & Chang, H.-H. & Chen, C. Low-Temperature Cu-Cu Bonding using Nanocrystalline Grains. in *2024 International Conference on Electronics Packaging (ICEP)*, Toyama, Japan: IEEE, Apr. 2024, pp. 109–110.
22. Hsiao, H.-Y. et al. Unidirectional Growth of Microbumps on (111)-Oriented and Nanotwinned Copper. *Science* **336**, 1007–1010 (2012).
23. Huang, Y.-S., Liu, C.-M., Chiu, W.-L. & Chen, C. Grain growth in electroplated (111)-oriented nanotwinned Cu. *Scr. Materialia* **89**, 5–8 (2014).
24. Tseng, H.-H. et al. Electroless-deposition of epitaxial (111)-oriented silver on nanotwinned copper microbumps for metal direct bonding. *J. Mater. Res. Technol.* **27**, 7957–7963 (2023).
25. Hong, Z.-J. et al. Room Temperature Cu-Cu Direct Bonding Using Wetting/Passivation Scheme for 3D Integration and Packaging. in *2022 IEEE Symposium on VLSI Technology and Circuits (VLSI*

Technology and Circuits), Honolulu, HI, USA: IEEE, June 2022, pp. 387–388.

26. Hsu, M.-P. et al. Enhancement of Low-Temperature Cu-Cu Bonding by Metal Alloy Passivation in Ambient Atmosphere. *IEEE Electron Device Lett.* **45**, 1500–1503 (2024).
27. Liu, D. et al. Low Temperature Cu/SiO2 Hybrid Bonding with Metal Passivation. in *2020 IEEE Symposium on VLSI Technology*, Honolulu, HI, USA: IEEE, June 2020, pp. 1–2.
28. Liu, D., Chen, P.-C., Liu, Y.-W., Hu, H.-W. & Chen, K.-N. Low-Temperature (70 °C) Cu-to-Cu Direct Bonding by Capping Metal Layers. *IEEE Electron Device Lett.* **42**, 1524–1527 (2021).
29. Aleshin, A. N., Bokstein, B. S., Egorov, V. K. & Kurkin, P. V. Grain Boundary and Bulk Diffusion in Au-Cu Thin Films. *DDF* **95–98**, 457–462 (1993).
30. Surholt, T., Mishin, Y.uM. & Herzig, C. hr Grain-boundary diffusion and segregation of gold in copper: Investigation in the type- *B* and type- *C* kinetic regimes. *Phys. Rev. B* **50**, 3577–3587 (1994).
31. Shie, K.-C., Gusak, A. M., Tu, K. N. & Chen, C. A kinetic model of copper-to-copper direct bonding under thermal compression. *J. Mater. Res. Technol.* **15**, 2332–2344 (2021).
32. Juang, J.-Y. et al. Copper-to-copper direct bonding on highly (111)-oriented nanotwinned copper in no-vacuum ambient. *Sci. Rep.* **8**, 13910 (2018).
33. Chen, K.-N., Fan, A. & Reif, R. Microstructure examination of copper wafer bonding. *J. Elec Mater.* **30**, 331–335 (2001).
34. Chen, K. N., Tan, C. S., Fan, A. & Reif, R. Morphology and Bond Strength of Copper Wafer Bonding. *Electrochem. Solid-State Lett.* **7**, G14 (2004).
35. Chen, K. N., Fan, A., Tan, C. S. & Reif, R. Temperature and duration effects on microstructure evolution during copper wafer bonding. *J. Elec Mater.* **32**, 1371–1374 (2003).
36. Kim, H. C., Alford, T. L. & Allee, D. R. Thickness dependence on the thermal stability of silver thin films. *Appl. Phys. Lett.* **81**, 4287–4289 (2002).
37. Lee, K.-P. et al. Mechanical strengthening of nanotwinned Cu films with Ag solid solution. *Mater. Lett.* **313**, 131775 (2022).
38. Li, W. & Chen, F. Optical, Raman and vibrational properties of closed shell Ag–Cu clusters from density functional theory: The influence of the atomic structure, exchange-correlation approximations and pseudopotentials. *Phys. B: Condens. Matter* **443**, 6–23 (2014).
39. Li, W. & Chen, F. Structural, electronic and optical properties of 7-atom Ag-Cu nanoclusters from density functional theory. *Eur. Phys. J. D.* **68**, 91 (2014).
40. Jia, Q. et al. Sintering mechanism of Ag-Pd nanoalloy film for power electronic packaging. *Appl. Surf. Sci.* **554**, 149579 (2021).
41. Jackson, M. S. & Che-yu, L. Stress relaxation and hillock growth in thin films. *Acta Metall.* **30**, 1993–2000 (1982).
42. Wang, H. Y., Najafabadi, R., Srolovitz, D. J. & Lesar, R. Interfacial segregation in Ag-Au, Au-Pd, and Cu-Ni alloys: I. (100) surfaces. *Interface Sci*. **1**, (1993). https://doi.org/10.1007/BF00203263.
43. Wang, Z.-J., Chen, J., Huang, Y. & Chen, Z.-X. Surface segregation of PdM (M=Cu, Ag, Au) alloys and its implication to acetylene hydrogenation, DFT-based Monte Carlo simulations. *Mater. Today Commun.* **28**, 102475 (2021).
44. Kagawa, Y. et al. An Advanced CuCu Hybrid Bonding For Novel Stacked CMOS Image Sensor. in *2018 IEEE 2nd Electron Devices Technology and Manufacturing Conference (EDTM)*, Kobe: IEEE, 2018, pp. 65–67.
45. Beyne, E. et al. Scalable, sub 2 μm pitch, Cu/SiCN to Cu/SiCN hybrid wafer-to-wafer bonding technology. in *2017 IEEE International Electron Devices Meeting (IEDM)*, San Francisco, CA, USA: IEEE, 2017, p. 32.4.1–32.4.4.
46. Murugesan, M. et al. Chip-to-Chip Hybrid Bonding with Larger-Oriented Cu Grains for μ-joints Beyond 100 K. in *2023 IEEE 73rd Electronic Components and Technology Conference (ECTC)*, Orlando, FL, USA: IEEE, 2023, pp. 1713–1718.
47. Wang, Y., Huang, Y.-T., Liu, Y. X., Feng, S.-P. & Huang, M. X. Thermal instability of nanocrystalline Cu enables Cu-Cu direct bonding in interconnects at low temperature. *Scr. Materialia* **220**, 114900 (2022).
48. Ong, J.-J. et al. Low-Temperature Cu/SiO2 Hybrid Bonding with Low Contact Resistance Using (111)-Oriented Cu Surfaces. *Materials* **15**, 1888 (2022).
49. Zhang, M., Gao, L.-Y., Li, J.-J., Sun, R. & Liu, Z.-Q. Characterization of Cu-Cu direct bonding in ambient atmosphere enabled using (111)-oriented nanotwinned-copper. *Mater. Chem. Phys.* **306**, 128089 (2023).
50. Ong, J. J., Shie, K.-C., Tu, K.-N. & Chen, C. Two-step fabrication process for die-to-die and die-to-wafer Cu-Cu bonds. in *2021 IEEE 71st Electronic Components and Technology Conference (ECTC)*, San Diego, CA, USA: IEEE, June 2021, pp. 203–210.
51. Tseng, H.-H. et al. Epitaxial Growth of (111) Nanotwinned Ag on (111) Nanotwinned Cu Films for Low-Temperature Cu–Cu Bonding. *Cryst. Growth Des.* **23**, 5519–5527 (2023).
52. Chen, C. et al. Low-temperature and low-pressure direct copper-to-copper bonding by highly (111)-oriented nanotwinned Cu. in *2016 Pan Pacific Microelectronics Symposium (Pan Pacific)*, Big Island, HI, USA: IEEE, Jan. 2016, pp. 1–5.

Acknowledgements

This work was financially supported by Center for Advanced Semiconductor Technology Research under Higher Education Sprout Project of Ministry of Education, Taiwan, the Co-creation Platform of the Industry Academia Innovation School, NYCU, under the framework of the National Key Fields Industry-University Cooperation and Skilled Personnel Training Act, and the National Science and Technology Council, Taiwan, under NSTC 112-2221-E-A49-163-MY3, NSTC 113-2221-E-A49-090-MY3, and NSTC T-Star Center Project: Future Semiconductor Technology Research Center under NSTC 114-2634-F-A49-001-.

Author contributions

Mu-Ping Hsu and Tai-Yu Lin conceived the study and designed the experiments. Hua-Jing Huang and Chiao-Yen Wang performed in-situ TEM and TEM measurements. Tsai-Fu Chung conducted TEM and 4D-STEM measurements and analyses. Wen-Wei Wu performed in-situ TEM and TEM measurements and provided optimization suggestions on experimental setup and data interpretation. Kuan-Neng Chen supervised the project and provided resources and funding. All authors discussed the results, contributed to manuscript revision, and approved the final version. Correspondence to Kuan-Neng Chen (knchen@nycu.edu.tw).

Competing interests

The authors declare no competing interests.

Additional information

Supplementary information The online version contains supplementary material available at https://doi.org/10.1038/s44172-025-00551-x.

Correspondence and requests for materials should be addressed to Kuan-Neng Chen.

Peer review information *Communications Engineering* thanks Mingxiang Chen, Chunjin Hang and the other, anonymous, reviewer(s) for their contribution to the peer review of this work. Handling Editors: [SungHoon Hur] and [Philip Coatsworth]. A peer review file is available.

Reprints and permissions information is available at http://www.nature.com/reprints

Publisher's note Springer Nature remains neutral with regard to jurisdictional claims in published maps and institutional affiliations.

Open Access This article is licensed under a Creative Commons Attribution-NonCommercial-NoDerivatives 4.0 International License, which permits any non-commercial use, sharing, distribution and reproduction in any medium or format, as long as you give appropriate credit to the original author(s) and the source, provide a link to the Creative Commons licence, and indicate if you modified the licensed material. You do not have permission under this licence to share adapted material derived from this article or parts of it. The images or other third party material in this article are included in the article's Creative Commons licence, unless indicated otherwise in a credit line to the material. If material is not included in the article's Creative Commons licence and your intended use is not permitted by statutory regulation or exceeds the permitted use, you will need to obtain permission directly from the copyright holder. To view a copy of this licence, visit http://creativecommons.org/licenses/by-nc-nd/4.0/.

© The Author(s) 2025